Geomorphology 273 (2016) 93–106

Contents lists available at ScienceDirect

Geomorphology

journal homepage: www.elsevier.com/locate/geomorph

Invited review

From hot rocks to glowing avalanches: Numerical modelling of gravity-induced pyroclastic density currents and hazard maps at the Stromboli volcano (Italy)

Teresa Salvatici [a,*], Alessio Di Roberto [b], Federico Di Traglia [a], Marina Bisson [b], Stefano Morelli [a], Francesco Fidolini [a], Antonella Bertagnini [b], Massimo Pompilio [b], Oldrich Hungr [c], Nicola Casagli [a]

[a] Dipartimento di Scienze della Terra, Università di Firenze, Via La Pira 4, 50121 Firenze, Italy
[b] Istituto Nazionale di Geofisica e Vulcanologia, Sezione di Pisa, Via della Faggiola 32, 56126 Pisa, Italy
[c] Department of Earth, Ocean and Atmospheric Sciences, University of British Columbia, Vancouver Campus, V6T 1Z4 Vancouver, Canada

ARTICLE INFO

Article history:
Received 30 October 2015
Received in revised form 1 August 2016
Accepted 5 August 2016
Available online 7 August 2016

Keywords:
Pyroclastic density currents
Geophysical flows modelling
Stromboli volcano
Hazard maps

ABSTRACT

Gravity-induced pyroclastic density currents (PDCs) can be produced by the collapse of volcanic crater rims or due to the gravitational instability of materials deposited in proximal areas during explosive activity. These types of PDCs, which are also known as "glowing avalanches", have been directly observed, and their deposits have been widely identified on the flanks of several volcanoes that are fed by mafic to intermediate magmas. In this research, the suitability of landslide numerical models for simulating gravity-induced PDCs to provide hazard assessments was tested. This work also presents the results of a back-analysis of three events that occurred in 1906, 1930 and 1944 at the Stromboli volcano by applying a depth-averaged 3D numerical code named DAN-3D. The model assumes a frictional internal rheology and a variable basal rheology (i.e., frictional, Voellmy and plastic). The numerical modelling was able to reproduce the gravity-induced PDCs' extension and deposit thicknesses to an order of magnitude of that reported in the literature. The best results when compared with field data were obtained using a Voellmy model with a frictional coefficient of $f = 0.19$ and a turbulence parameter $\xi = 1000\ m\ s^{-1}$. The results highlight the suitability of this numerical code, which is generally used for landslides, to reproduce the destructive potential of these events in volcanic environments and to obtain information on hazards connected with explosive-related, mass-wasting phenomena in Stromboli Island and at volcanic systems characterized by similar phenomena.

Contents

* Corresponding author.
E-mail address: teresa.salvatici@unifi.it (T. Salvatici).

http://dx.doi.org/10.1016/j.geomorph.2016.08.011

1. Introduction

Glowing avalanches generated from the collapse of the unstable portion of a volcanic crater's rim or the gravitational instability of materials deposited during explosive activity can be defined as gravity-induced pyroclastic density currents (PDCs). They have been directly observed and their deposits have been identified on the flanks of several volcanoes fed by mafic to intermediate magmas (Davies et al., 1978; Nairn and Self, 1978; Hazlett et al., 1991; Arrighi et al., 2001; Alvarado and Soto, 2002; Calvari and Pinkerton, 2002; Cole et al., 2005; Yasui and Koyaguchi, 2004; Yamamoto et al., 2005; Miyabuchi et al., 2006; Behncke et al., 2008; Di Roberto et al., 2014; Di Traglia et al., 2014; Calvari et al., 2016). Such gravity-induced PDCs have small volumes (10^4–10^7 m^3) but are emplaced at very high temperatures and can travel far from the source (Davies et al., 1978; Nairn and Self, 1978; Hazlett et al., 1991; Yamamoto et al., 2005; Miyabuchi et al., 2006; Di Roberto et al., 2014). Small volume PDCs are potentially dangerous for communities close to the volcanoes and tourists. Runouts longer than 8 km from the source have been reported for gravity-induced PDCs that presumably resulted from the avalanching of pyroclastic materials accumulated on slopes steeper than the angle of repose at Shin-Fuji volcano, Japan (Yamamoto et al., 2005) and for those that emerged from notches in the crater rim during the 1974 eruption of the Fuego volcano, Guatemala (Davies et al., 1978). Similar "gravity-induced" processes have been hypothesized for the formation of the glowing avalanches generated during the 1975 eruption at Ngauruhoe volcano, New Zealand (Nairn and Self, 1978; Lube et al., 2007) and for the PDCs of Asama volcano, Japan (Aramaki and Takahashi, 1992; Yasui and Koyaguchi, 2004) and Tungurahua volcano, Ecuador (Kelfoun et al., 2009). On 11 February 2014, a large volume of unstable and hot rocks detached from the lower-eastern flank of Etna's New Southeast Crater, Italy, and caused a PDC, travelling approximately 3 km on the eastern flank of the volcano and reaching the bottom of Valle del Bove at an average speed of >60 km h^{-1} (Bonforte and Guglielmino, 2015; De Beni et al., 2015). In addition, there are more hazards connected with small-volume gravity-induced PDCs. To improve hazard assessments from all types of PDCs, it is necessary to expand the understanding of PDCs and evaluate their possible impacts on human activities.

In this research, the suitability of landslide numerical models for simulating and assessing hazards related to gravity-induced PDCs was tested. The results of a back-analysis of three events of "glowing avalanches" at the Stromboli volcano are presented. The DAN-3D depth-averaged 3D numerical code, developed by McDougall and Hungr (2004) and Hungr and McDougall (2009), was applied. As case studies, three gravity-induced PDCs in 1906, 1930 and 1944 were selected. In relation to the 1930 event, detailed descriptions were compiled by Rittmann (1931) and Abbruzzese (1935) shortly after the eruption, from which crucial parameters such as the total runout distance, velocity, thickness and distribution of the deposits were deduced. Additional data on the flow dynamics and distributions of the deposits have been reported by Di Roberto et al. (2014).

The findings were also used to assess whether the inhabited areas of Stromboli (Stromboli and Ginostra villages) could be affected if one of the events is repeated in the future with dynamics similar to that in historical times and to evaluate the potential associated damage. The methodology used here may be applied to other volcanoes and, perhaps to other geological contexts, giving implications for hazard assessments in areas prone to mass-flows.

2. Eruptive activity and pyroclastic flows at the Stromboli volcano

Stromboli is the northernmost volcanic island of the Aeolian archipelago, in the southern Tyrrhenian Sea (Fig. 1). The island is the subaerial part of a rather regular volcanic edifice that rises to 924 m above sea level (a.s.l.) from a base that lies at a water depth between 1300 and 2300 m. Volcanic activity on Stromboli has been continuous since the III–VII centuries A.D. and consists of mild- to low-energy intermittent explosions (Strombolian activity), which are occasionally interrupted by effusive events and violent explosions that are commonly called paroxysms (Barberi et al., 1993; Rosi et al., 2000). The active vents are located in the crater terrace at approximately 750 m a.s.l. on the upper part of the Sciara del Fuoco (SdF), which is a horseshoe-shaped depression on the NW uninhabited flank of the volcano (Fig. 1).

At the Stromboli volcano, the formation of mass flows of hot pyroclasts has been reported several times. The flows occurred as a direct result of explosive and effusive volcanic activities such as those on 6 December 1985, (De Fino et al., 1988), 5 April 2003, (Rosi et al., 2006, accepted for publication; Pistolesi et al., 2008) and 12 January 2013 (Di Traglia et al., 2014; Calvari et al., 2016) or of the sliding of incandescent pyroclastic fall deposits accumulated over steep slopes such as during the 1930 and 1944 paroxysms (Di Roberto et al., 2014) and the eruptive activity of 28 and 29 December 2002 (Pioli et al., 2008). Gravity-induced PDCs usually occur in the SdF depression and therefore do not represent a serious threat to the population of Stromboli (Barberi et al., 1993; Rosi et al., accepted for publication). However, in 1906, 1930 and 1944, gravity-induced PDCs occurred outside the SdF, and in the latter two cases they reached the coast of the island. In particular, the 1930 PDCs reached the village of Stromboli on the NE part of the island, causing extensive damage and four casualties (Rittmann, 1931).

2.1. Gravity-induced PDCs in 1906, 1930 and 1944

Little information was reported on the PDCs on 15 July 1906 and 20 August 1944. Riccò (1907) reported that during the late afternoon of 15 July 1906 a very large eruption of incandescent material hit the area of Forgia Vecchia on the ESE side of the island (Fig. 1) and was preceded by a loud and long-lasting rumble. A column of incandescent material flowed in the direction of the village of Ginostra, WSW from the vent, burning the vegetation. Similarly, Ponte (1948) described that on 20 August 1944 a large amount of incandescent material consisting of large blocks and ash that had accumulated on the summit of the volcano and on the Forgia Vecchia flowed downslope, reached the shore and formed a ca. 100-m-long delta in the sea. The delta was rapidly eroded by the action of sea waves.

The event during the 1930 paroxysm is the best described. It was triggered by the sliding of an approximately 1 m-thick source deposit with an estimated volume of at least 45,000 m^3 and consisting of metre-sized spatters, decimetre-sized bombs, lapilli, and ash (Rittmann, 1931; Abbruzzese, 1935). That deposit had accumulated over an area of >60,000 m^2 on the steep cliff side of Chiappe Lisce (Fig. 1) approximately 1 h before the initiation of the gravity-induced PDC event (Rittmann, 1931) during an extremely violent paroxysm; this paroxysm was possibly the most violent event known to date in the recent history of Stromboli (Bertagnini et al., 2011). The initiation mechanism can be classified as a "rock irregular slide", which is defined as the "sliding of a rock mass on an irregular rupture surface consisting of a number of randomly oriented joints, separated by segments of intact rock" (Hungr et al., 2014). The failure mechanism of this type of landslide is generally complex and difficult to describe and often includes elements of toppling (Hungr et al., 2014). At Stromboli, the inclination of some slopes exceeds the internal friction angle of the pyroclastic materials, but this condition is not sufficient to induce "rock irregular slide" events (Nolesini et al., 2013). Instead, the sliding processes are induced by the accumulation of pyroclastic materials, which produces a loading effect (overloading) on the summit of the volcano (Nolesini et al., 2013). This mechanism was also proposed for the generation of the glowing avalanches at Mt. Vesuvius during the 1944 eruption (Hazlett et al., 1991). Analogue modelling by Nolesini et al. (2013) revealed that the accumulation of material (representing either lava or spatter

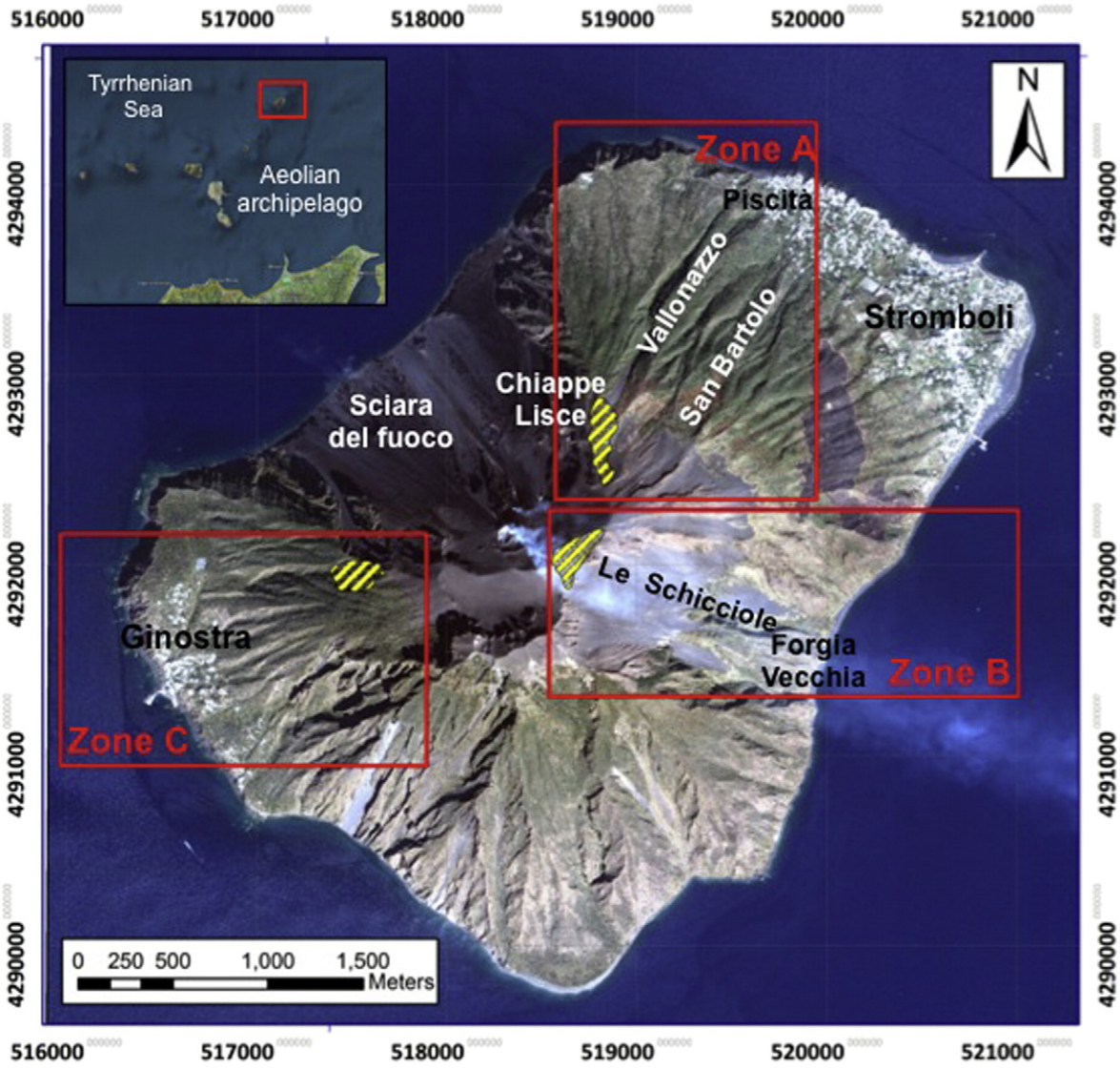

Fig. 1. Orthoimage of the study area, Stromboli volcano with the primary toponyms (from the QuickBird Satellite Sensor). The three red rectangular areas cover the volcanic sectors involved in the gravity-induced PDCs of 1930 (zone A), 1944 (zone B) and 1906 (zone C). These zones were used for numerical modelling with DAN-3D. The source areas of the three events are shown by yellow hatches.

agglutinates) overcomes slope stability, generates complex systems of landslides and increases the volume of material involved in the sliding processes.

The phenomenon begins with instability in the lower part of the slope on which material accumulates which results in a remobilization of the deposited material in a landslide (Fig. 2a). This mechanism for generating gravity-induced PDCs is consistent with the model proposed by Ui et al. (1999) and Takahashi and Tsujimoto (2000) for the dome collapse-induced block and ash flows (Merapi-type) during the 1991–1995 eruption of Unzen Volcano, Japan.

Failures of crater-rims or pyroclastic piles develop into rockslides, dry gravel/debris flows or avalanches (Hazlett et al., 1991; Cole et al., 2005; Di Traglia et al., 2014), which have been described as the "extremely rapid, massive, flow-like motion of fragmented rock from a large rock slide or rock fall" (Hungr et al., 2014). Rockslides attain a degree of mobility that far exceeds what would be expected from a frictional flow of dry, angular, broken rock, and the mobility is increased with the volume of an event (Heim, 1932; Hayashi and Self, 1992; Dade and Huppert, 1998; Calder et al., 1999).

2.2. Description of the deposits

The deposits related to the 1930 event, including grain-size and componentry were described in Di Roberto et al. (2014). The deposits of the 1930 paroxysms comprise of 1) a spatter bomb deposit and 2) a fallout deposit. Spatter deposits crop out on both sides of the Sciara del Fuoco down to 120 m a.s.l. in an area that extends to some hundreds metres apart from both margins of the depression. Below 400 m a.s.l., the deposit consists of up to 4 m^2-sized, single to agglutinated, ribbon to convoluted spatter bombs up to 50 cm in length, which often laterally pass to alignments of flattened pumice and scoria bombs with centimetres to decimetres sizes. Moving upslope on the volcano, the spatter deposit becomes more and more continuous, and above 400 m a.s.l., it crops out as a decimetre-thick, nearly continuous accumulation.

At the base of the spatter deposit, a pyroclastic fallout deposit of coarse ash to medium lapilli ($Md\Phi = 0.8–2.5$) occurs, with thickness of a few to ca. 20 cm and consists of fresh, light coloured pumice, glassy black scoriae, and variable amounts of lithic fragments.

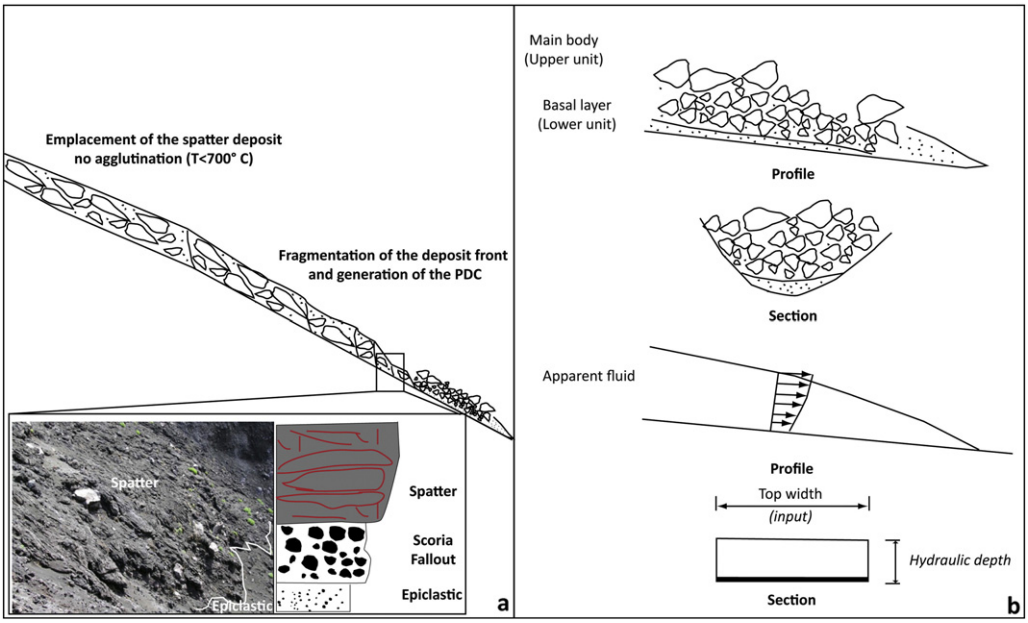

Fig. 2. The model approach a) Generation of gravity-induced PDCs at the Stromboli volcano through the sliding of spatter blankets accumulated during paroxysmal explosions. b) "Equivalent-fluid" simplified approach for the simulation of mass flow motion used in DAN-3D (Hungr, 1995; Hungr and McDougall, 2009). The momentum equations evaluate the internal frictional rheology, which is governed by an internal friction angle and by a basal rheology that is chosen by the operator according to one of seven rheological functions: frictional, plastic, Newtonian, turbulent, Bingham, Coulomb frictional and Voellmy.

The most complete outcrop of the 1930 PDC occurs at the opening of the S. Bartolo Valley, at approximately 420 m a.s.l. The thickness of the PDC deposits there is >4.5 m, and the base is not exposed. The deposit rapidly thins downslope, and 75 m away from the main outcrop it is ca. 2 m-thick. This order of magnitude of the thickness (approximately 1.5 m) remains to the end of the Vallonazzo where the PDC stopped.

The PDC deposit consists of two main units. The lower unit is a ~10 to 20 cm-thick, well-sorted medium ash, with $\sigma\phi = 1.27$ (sorting, with ϕ is the negative log base 2 of the grain diameter), $Md\phi = 1.63$ (median diameter) and $F1 = 72.20$ (wt.% of material, <1 mm). Lower unit often exhibits parallel to low-angle cross-laminations and short alignments of centimetric lapilli. The components include juvenile scoriae and pumices, which constitute 73 vol.% and show subrounded shapes and incipient surficial abrasion. Lithics, which represent 27 vol.% of the deposit, are concentrated mainly in the finest grain sizes and consist of reddish, holocrystalline subvolcanic rocks; orange-coloured, palagonitized or altered glassy scoriae; and loose magmatic crystals (plagioclase, clinopyroxene and olivine).

The upper unit ($\sigma\phi = 5.09$, $Md\phi = -0.79$, and $F1 = 31.19$) is constituted by metre-sized lithic blocks and bombs, multi decimetre to centimetre-sized juvenile scoriae, and pumices supported by a poorly sorted, massive, coarse ash matrix. The larger blocks are often aligned in the direction of flow and are concentrated on the uppermost part of the deposit.

3. Methods

3.1. Model description

In accordance with the failure mechanism and motion of the Stromboli PDCs, the suitability of the DAN-3D depth-averaged numerical code (McDougall and Hungr, 2004; Hungr and McDougall, 2009) was tested. The code is commonly used in landslide modelling to simulate and assess hazards related to gravity-induced flows. In addition, DAN-3D has been commonly and effectively used for the simulation of volcanic debris avalanches (Morelli et al., 2010; Sosio et al., 2012a) and other landslides in which the dominant process is represented by grain collisions (McDougall and Hungr, 2004; Sosio et al., 2008; Hungr and McDougall, 2009; Sosio et al., 2012b). The numerical code assumes a simplified "equivalent-fluid" approach for the simulation of mass-flow motion (Fig. 2b; Hungr, 1995; Hungr and McDougall, 2009). Starting from the theory of Savage and Hutter (1989); Hungr (1995) proposed

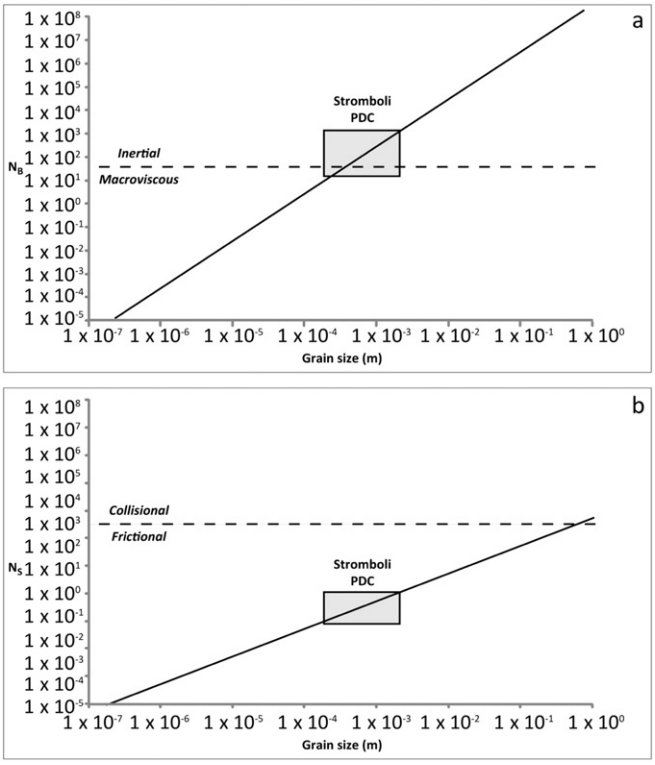

Fig. 3. The numbers to understand the dynamic regime of granular flows a) Bagnold number and b) Savage number estimations for the 1930 Stromboli gravity-induced PDC, based on grain-size data reported by Di Roberto et al. (2014). Although the PDC was at the inertial and macroviscous border for the Bagnold number, the Savage number estimation revealed a frictional behaviour that supports the assumption of internal frictional behaviour used in the DAN-3D model.

Table 1
Main characteristics of the three events. Zones A, B, and C are from Rittmann (1931), Abbruzzese (1935) and Di Roberto et al. (2014).

	Zone A	Zone B	Zone C
Eruption	1930	1944	1906
Date	Sept 11	Jun 15 (uncertain)	Aug 20
Area of interest	NE flank	WSW flank	ESE flank
Source elevation (m a.s.l.)	790	920	600
Volume source (m^3)	42,000	35,000	33,000
Entrainment (Mm^3)	Unspecified	Unspecified	Unspecified
Travel distance (km)	1.6	1.5	–
Thickness (m)	0.1–4	0.1–0.6	–
Velocity ($m\ s^{-1}$)	15–20	–	–
H/L (height/run out distance)	<0.4	<0.5	–

a semi-empirical approach in which the heterogeneous flowing material was modelled as a hypothetical material governed by two simple rheological relationships, one for the base and the other for the inner part, which may differ from each other. The idea of the separation of internal and basal friction mechanisms has its roots in the depth-integrated solutions of classical fluid dynamics, where a variety of viscous or turbulent relationships can be used to determine basal friction forces of a flowing sheet of fluid, whereas the internal stress distribution is assumed to be hydrostatic (e.g., Chow, 1959; Savage and Hutter, 1989; Hungr and McDougall, 2009).

Many published papers have confirmed the validity of Coulomb's (1776) model of rate-independent frictional deformation in modelling PDCs as granular materials (Iverson and Denlinger, 2001; Widiwijayanti et al., 2009; Procter et al., 2010; Sulpizio et al., 2010a; Charbonnier and Gertisser, 2012). The assumption of a frictional internal rheology is based on the dynamic regime of granular flows that can be expressed by two major non-dimensional numbers: the Bagnold number (N_B) and the Savage number (N_S). The former characterizes the relative importance of the interstitial fluid to the transport of momentum and can be formulated as (Bagnold, 1954; Iverson and Denlinger, 2001; Bursik et al., 2005):

$$N_b = \left(\frac{C_s}{C_*^{1/3} C_s^{1/3}}\right)^{1/2} \frac{\rho_s \gamma d^2}{\mu} \tag{1}$$

where C_s is the volumetric particle concentration in the flow (=0.5, as suggested by Iverson and Denlinger, 2001), C is the particle density at maximum packing (=0.7; Iverson and Denlinger, 2001), ρ_S is the particle density ($\rho_S = 1.08 \times 10^3\ kg\ m^{-3}$; Apuani et al., 2005a), γ is the strain rate (=10; Iverson and Denlinger, 2001), d is the typical particle diameter (in the range measured by Di Roberto et al., 2014, see Section 2.2), and μ is the dynamic viscosity of the interstitial fluid ($=3.5 \times 10^{-5}$, Iverson and Denlinger, 2001). The bracketed term in (1) shows the influence of the grain concentration C_s on the stress regime. For $N_B \le 40$, the material is in the macroviscous regime, in which the interstitial fluid plays a significant role in momentum transfer, but probably only under extreme unusual circumstances (very fine-rich flows), where the bulk behaviour of a volcanic granular flow would be macroviscous (Bursik et al., 2005). Otherwise, for $N_B \ge 450$, the flow behaviour is supposed to be inertial, i.e., momentum transport is by interparticle interactions (Bursik et al., 2005).

The Savage number, which characterizes the relative importance of momentum transfer by interparticle collisions to that by inter-particle friction, can be expressed as

$$N_s = \frac{\rho_s \gamma^2 d^2}{(\rho_s - \rho) g z}, \tag{2}$$

where ρ is the density of the interstitial fluid (=6; Iverson and Denlinger, 2001), g is the gravitational acceleration, and z is a slope perpendicular coordinate measured from the flow surface down. Approximately, N_S represents the ratio of grain collision stresses to Coulomb friction produced by grain contact stresses (Iverson and Denlinger, 2001). The collisional regime ($N_S \ge 0.1$) characterizes flows where grain collisions may be important to momentum transfer, and shear stress depends on strain rate, as in a fluid (diluted granular flows; e.g., Bursik et al., 2005). Otherwise, the flow is in the frictional regime (Bursik et al., 2005). The presence of intergranular pore-fluid pressure influences Coulomb friction in deforming granular masses, but only if high fluid pressures produce complete mixture fluidization, simulating the condition $\rho_S = \rho$ (Bagnold, 1954; Iverson and Denlinger, 2001). However, regardless of the shear rate or degree of dilatation, the Coulomb equation adequately describes bulk intergranular shear stresses produced in response to the slope-parallel member of the mixture weight (Iverson and Denlinger, 2001).

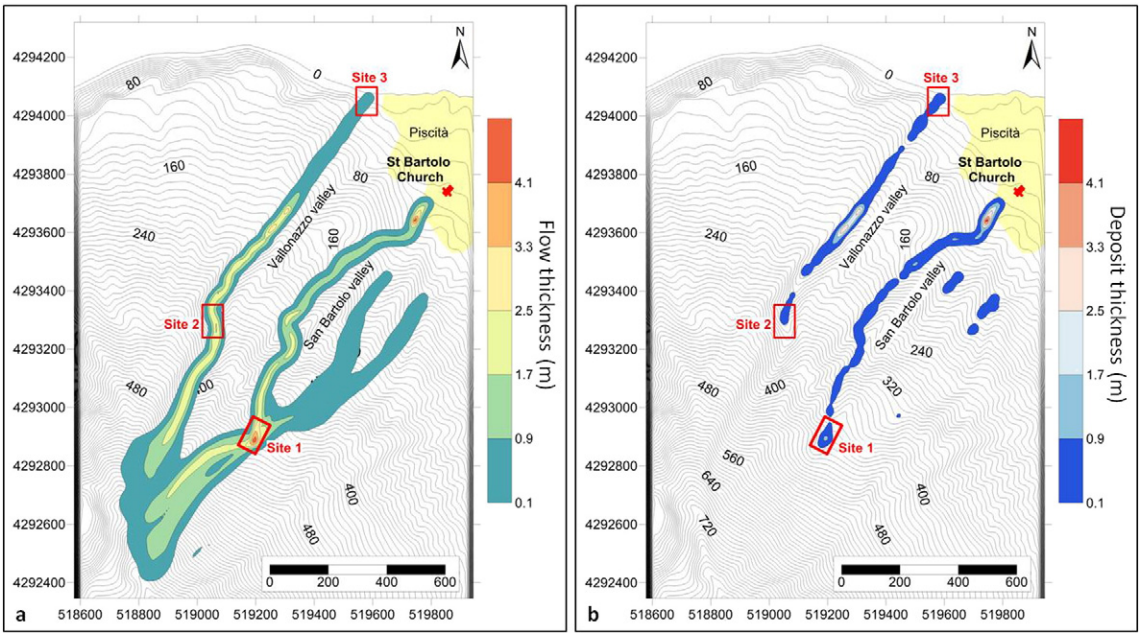

Fig. 4. Results of the DAN-3D simulation with the non-modified input thickness: a) flow thickness and b) deposit thickness after an interval of 135 s for zone A (1930-like event).

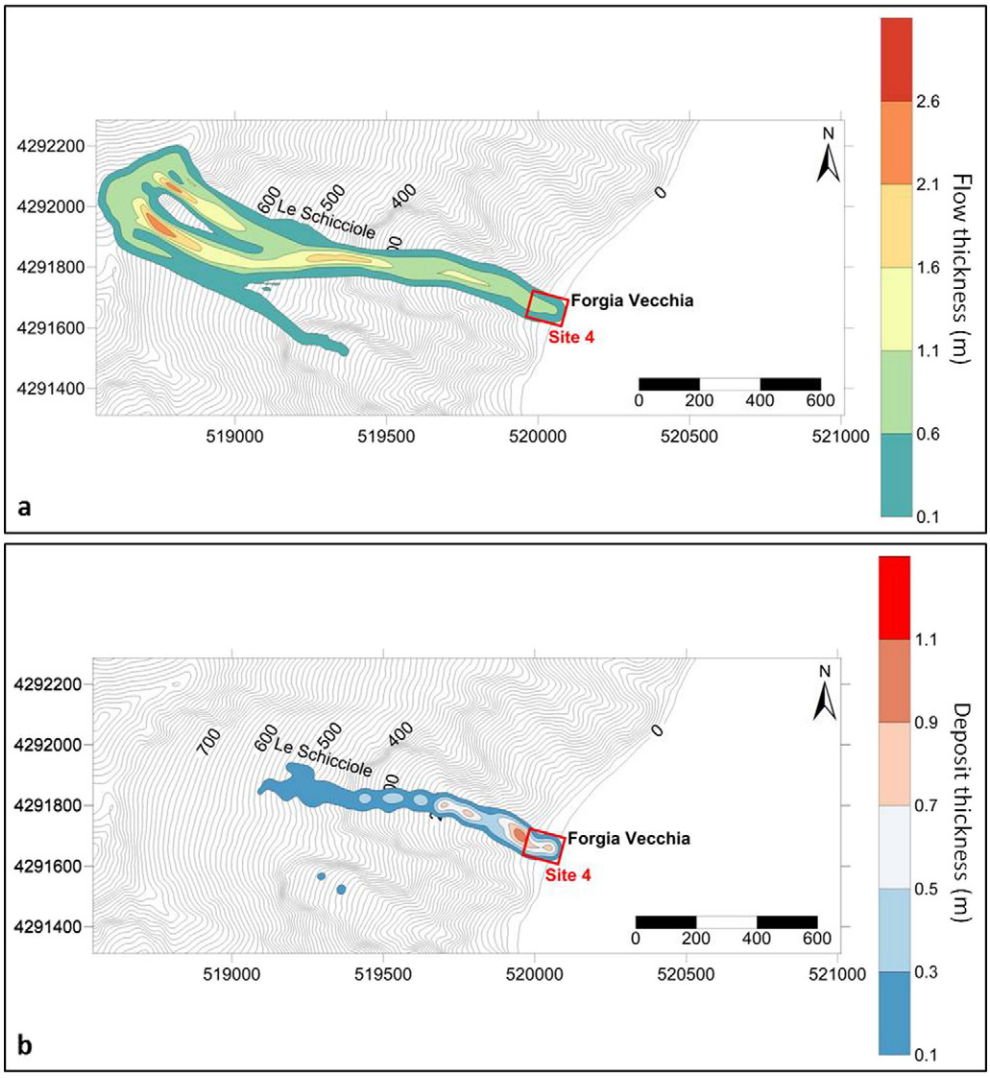

Fig. 5. Results of the DAN-3D simulation with the non-modified input thickness: a) flow thickness and b) deposit thickness after an interval of 88 s for zone B (1944-like event).

Based on the grain-size data reported in Di Roberto et al. (2014), the Stromboli gravity-induced PDCs fall on the border between the macroviscous and inertial regime (Fig. 3a) and in the frictional regime field (Fig. 3b).

DAN-3D uses the Lagrangian numerical method to solve the depth-average integrated St. Venant equations adapted from Smoothed Particle Hydrodynamics (SPH) (Monaghan, 1989, 1992; Benz, 1990). The model is divided into an internal frictional rheology that is governed by an internal friction angle and a basal rheology that is chosen by the operator according to one of seven rheological kernels implemented in the numerical code (Hungr, 1995): frictional, plastic, Newtonian, turbulent, Bingham, power law and Voellmy. A detailed description of the model was reported by Hungr and McDougall (2009).

3.2. Model calibration and input data for simulation

Simulations were performed on three areas corresponding to those affected by the gravity-induced PDCs of 1930 (zone A), 1944 (zone B) and the area possibly affected in the 1906 event (zone C) (Fig. 1). Zone A was used as a test area because information on the distributions and thickness of deposits, the velocity of the 1930 glowing avalanche, the event duration and the total travel distance are known from the literature (Rittmann, 1931; Abbruzzese, 1935; Di Roberto et al., 2014).

The materials involved in 1906 and 1944 gravity-induced PDCs were assumed to be similar to that of 1930 (for example, see Bertagnini et al., 2011). Thus, the parameters obtained for zone A were used to calibrate the model by back-analysis and to find the input rheological parameters that were later applied to the simulations in zones B and C. The main characteristics of the three events under consideration are shown in Table 1.

The modelling was performed on a high resolution (50 cm) Digital Elevation Model (DEM) of the current volcanic flank. The DEM was obtained by elaborating the 3D data (8 points m^{-2}) acquired during the airborne laser scanning survey on 04 May 2012 to 18 May 2012 carried out by the BLOM Compagnia Generale Ripreseaeree S.P.A. (www.blomasa.com).

The construction period and resolution of the DEM are important issues when testing the accuracy of any terrain-dependent model, and, in this case, the exact reconstruction of the pre-event topography is difficult. We used the current topography assuming that it well approximates the topography before the avalanche. Most of the materials deposited by the pyroclastic flow have been eroded, and only limited portions are preserved in sheltered areas, and, therefore, the topography is largely unchanged compared to that of 1930. Because DAN-3D does not work correctly with path grids that are excessively detailed, the path grid file was resampled to a spatial resolution of 5 m and repeatedly filtered using Gaussian smoothing (3 × 3). The use of the

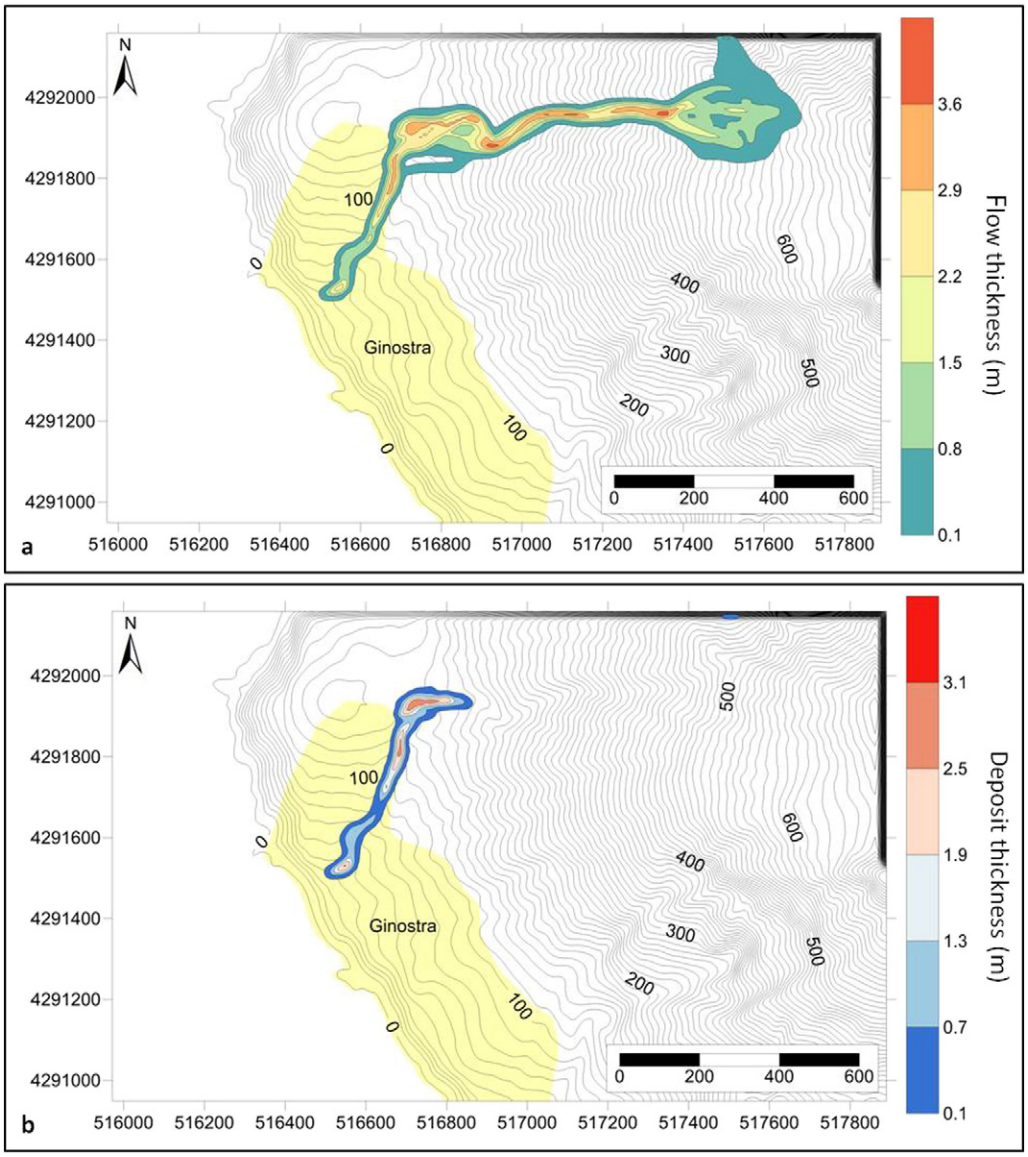

Fig. 6. Results of the DAN-3D simulation with the non-modified input thickness: a) flow thickness and b) deposit thickness after an interval of 180 s for zone C (1906-like event).

Smoothed Particle Hydrodynamics (SPH) numerical technique allowed the slide materials to spread, branch and join without problems due to the mesh and flow boundaries (McDougall and Hungr, 2003).

The area where accumulations of spatter and fallout deposits were observed (Rittmann, 1931) was assumed to be the source area of the 1930 gravity-induced PDC, whereas for the 1906 and 1944 eruptions, the source areas were identified as the regions upslope of the flow path where the slope exceeds 29° (Di Roberto et al., 2014). This value is usually assumed to be the lowermost value of the angle of repose for dry pyroclastic deposits (Apuani et al., 2005b; Miyabuchi et al., 2005). The initial value of 1 m for the thickness of the sliding material was defined according to the observations by Rittmann (1931) regarding the material accumulated on the summit of the volcano shortly before the 1930 PDC. The value was then applied to the other two events. The source volumes reconstructed using those areas and material thicknesses are reported in Table 1.

Erosion was not considered because a very low degree of substrate erosion and entrainment was observed in the field and defined by a sedimentological study of the 1930 event deposits (Di Roberto et al., 2014).

Because DAN-3D does not implement a routine for automatically stopping the simulation, we decided to interrupt the simulation when the flow reached sea level. If the flow never reached the coastline, the simulation was manually stopped when the flow velocity decreased to zero.

Finally, to provide a useful contribution to the assessment of hazards associated with gravity-induced PDCs at Stromboli, a further set of simulations with doubled thicknesses of the source deposits was also performed (double volume). The corresponding potential event could be considered a worst-case scenario for the inhabited areas of Stromboli Island.

4. Results

The simulations relative to the 1930 PDC were performed with frictional, plastic and Voellmy rheologies by a trial-and-error procedure (Morelli et al., 2010; Sosio et al., 2012a, 2012b). This method was used to obtain values of the runout, velocity, and duration of the flow that will match those derived from the literature and the available field data. The simulation that best reproduced the path, extension, and thickness order of magnitude of the 1930 gravity-induced PDC deposit (zone A) was obtained using a Voellmy rheological model with a frictional coefficient of $f = 0.19$, a turbulence parameter $\xi = 1000\ \mathrm{m\ s^{-2}}$, a unit weight of 14.71 and an internal friction angle of $\phi_i = 20°$ (Apuani et al., 2005b). That rheology

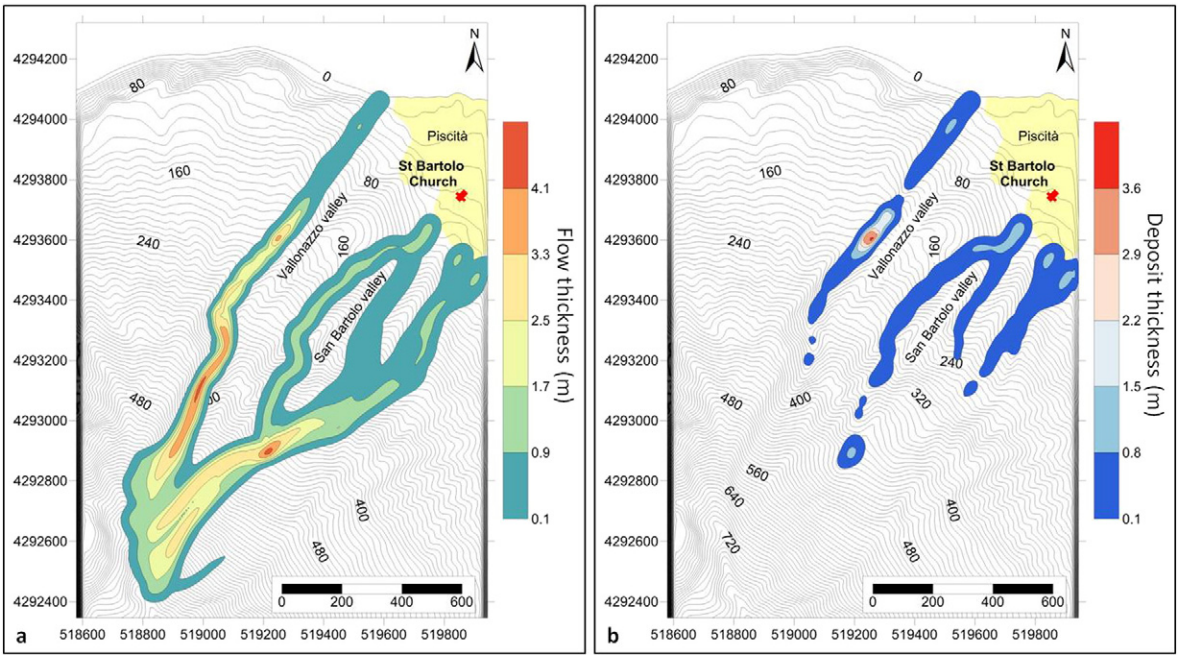

Fig. 7. Results of the DAN-3D simulation using a double input thickness: a) flow thickness and b) deposit thickness after an interval of 90 s for zone A (1930-like event).

matched the frictional and turbulent behaviours and allowed a better description of the complex dynamics of the avalanche and its long travel distance.

Simulations using the Voellmy rheological model displayed a strong topographic control, which allowed the 1930-like gravity-induced PDCs to flow inside the Vallonazzo valley with little overbank deposition. The Voellmy rheology differs from the simple Coulomb-type friction law by the presence of a turbulent component in addition to the frictional component ξ (Sosio et al., 2012a, 2012b). This component aids the flow resistance, which depends on the square of the velocity, by incorporating a coefficient that is used to represent the effects of turbulence and/or collisions (Kelfoun et al., 2010). The main parameters used during the back-analysis to constrain the model results were the flow length, impact area along the valley and the runout time. Historical accounts and field data (Abbruzzese, 1935) revealed that during the 1930 event "… flows of incandescent material were sliding into the S. Bartolo and Piscità (Vallonazzo) valleys. The first one stopped within tens of metres from the church of S. Bartolo (where the slope change from 25° to 15°), whereas the second one reached the sea". The simulation using the Voellmy rheological model was able to reproduce the two main gravity-induced PDCs reported in the literature (Rittmann, 1931; Abbruzzese, 1935; Di Roberto et al., 2014); the first flow extended along the Vallonazzo valley and reached the sea close to Piscità after 135 s, and the second flow moved in the San Bartolo valley and stopped near the church of San Bartolo after approximately 120 s (Fig. 4a).

The Voellmy rheological model also simulated the 1930 PDC deposits' thicknesses, matching the order of magnitude of those measured in the field by Di Roberto et al. (2014). At approximately 418 m a.s.l. in the San Bartolo valley (Site 1 of Di Roberto et al., 2014; Fig. 4b) the measured thickness was approximately 4.5 m, and the simulated thickness was 1.6 m. In the NE rim of the Vallonazzo valley, at approximately 370 m a.s.l. (Site 2 of Di Roberto et al., 2014; Fig. 4b), the measured and simulated thicknesses were comparable and had accuracies of 30–40 cm, whereas close to the outlet of Vallonazzo valley (Site 3 of Di Roberto et al., 2014; Fig. 4b), the measured thickness was approximately 100 cm, and the simulated thickness was 60 cm. The areas hit by the gravity-induced PDC and covered by the deposit were 3.6×10^5 and 0.8×10^5 m^2, respectively.

Comparatively, the frictional basal rheologies with friction angles between 20°–25° and shear strength between 2 and 5 kPa) basal allowed the simulation of 1930-like gravity-induced PDCs. The low topographic control produced over-estimates of lateral spread and velocity of the flow, whereas the thickness was under-estimated. Similar results were obtained by Sosio et al. (2012a), who modelled volcanic debris avalanches using DAN-3D. Frictional rheology assumes that emplacement is controlled by path topography. Deposition is strongly slope-dependent, and material therefore flows at any gradient greater than the basal friction angle (Sosio et al., 2012a). The plastic basal rheology (yield stress fluid) depends on the shear stress applied to its basal level, regardless of its thickness and velocity (Kelfoun, 2011), which does not allow for strong topographic control like the 1930 gravity-induced PDC.

The rheological parameters obtained using this procedure for the 1930 PDC were then used in the simulation of the gravity-induced PDCs events in zones B (in 1944) and C (in 1906). The results for zone B show that the flow moved into the "Le Schicciole" valley (Forgia Vecchia) and reached the sea in 88 s. In this case, the simulated deposit thickness of 60 cm matched the field measurement (Fig. 5; Di Roberto et al., 2014). The areas impacted by the PDC and covered by the deposit in zone B were 3.1×10^5 and 0.8×10^5 m^2, respectively.

The simulation in zone C showed that the flow never reached the sea (Fig. 6). After an initial phase of spreading on the flat area above the village of Ginostra, the flow channelized inside the village and stopped after approximately 180 s. In this case, no data in the literature describe the flow dynamics and runout or the deposit's thickness, and a direct comparison between the results of the simulation and field evidence was impossible. In zone C, the areas impacted by the PDC and covered by the deposit were 1.5×10^5 and 0.3×10^5 m^2, respectively.

A second set of simulations was performed in the same areas. In these simulations we arbitrarily used a source deposit with double thickness compared to previous simulations, i.e. a double volume of materials involved in the flow. A paroxysm able to emplace a thickness of deposit double respect to those emplaced in 1930 possibly represents the worst scenario for the generation of a gravity-

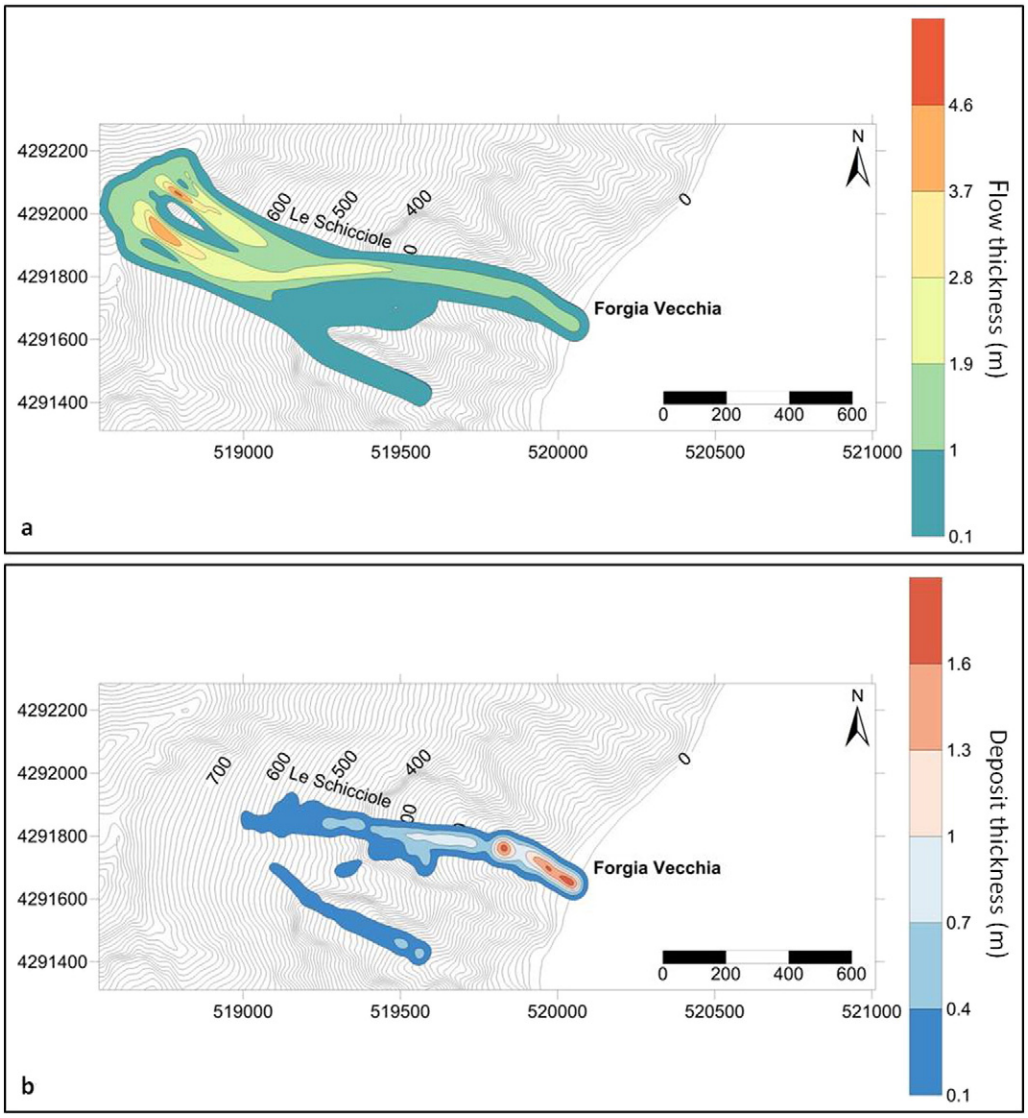

Fig. 8. Results of the DAN-3D simulation with a double input thickness: a) flow thickness and b) deposit thickness after an interval of 70 s for zone B (1944-like event).

induced PDC on the Stromboli volcano. The results show that areas impacted by double volume PDCs are larger than those affected during the first simulation. In particular, in zone A, the flow reached the Piscità locality after approximately 90 s and moved into the San Bartolo valley and adjacent valleys, depositing material along its path. The deposits were more distributed and reached a maximum thickness of 3.8 m in the Vallonazzo valley (Fig. 7). The areas impacted by the gravity-induced PDC and covered by the deposit in the simulation with the double initial thickness were 5.6×10^5 and 1.3×10^5 m^2, respectively.

The simulation in zone B showed that deposition still occurred in the "Le Schicciole" valley (Forgia Vecchia), but it also occurred in the adjacent valley. In this case, the flow front reached the coastline after approximately 70 s (Fig. 8). The areas impacted by the gravity-induced PDC and covered by the deposit in the simulation with a double initial thickness in zone B were 4.1×10^5 and 1.6×10^5 m^2, respectively.

In zone C, the flow ran through Ginostra village and reached sea level after approximately 100 s, with little lateral expansion in the urbanized areas. The deposit's maximum thickness was 4.4 m (Fig. 9). The areas impacted by the PDC and covered by the deposit according to the simulation with the double initial thickness were 1.9×10^5 and 0.5×10^5 m^2, respectively.

In the simulation with double volume, the travel times of the flows in areas A, B and C decreased by 30%, 20% and 44%, respectively. The increase in volume caused consistent increase in the flow velocity and a greater impact force of the flow.

5. Discussion

5.1. Evaluation of modelling results

The best-fit rheologies (internal friction and basal friction/turbulent) well explained the 1930 PDC deposits, especially in the upper part of the deposit, which consists of a "blocks/bombs-and-ash-flow" (Miyabuchi et al., 2006) with metre to centimetre-sized clasts supported by a poorly sorted, massive, coarse ash matrix. This deposit is similar to the small-volume block-and-ash flows and rockfalls during the Soufriere Hills eruption (Cole et al., 2002) and the small-volume PDCs during the 1975 eruption at Ngauruhoe (Nairn and Self, 1978), which were interpreted as inertial granular flows (Lube et al., 2007). The lower unit consists of tens of cm-thick, well-sorted, medium ash deposit that often exhibit parallel to low-angle cross-laminations and short alignments of centimetric lapilli, which are in good agreement with the basal friction + turbulent rheology described by the Voellmy rheological model.

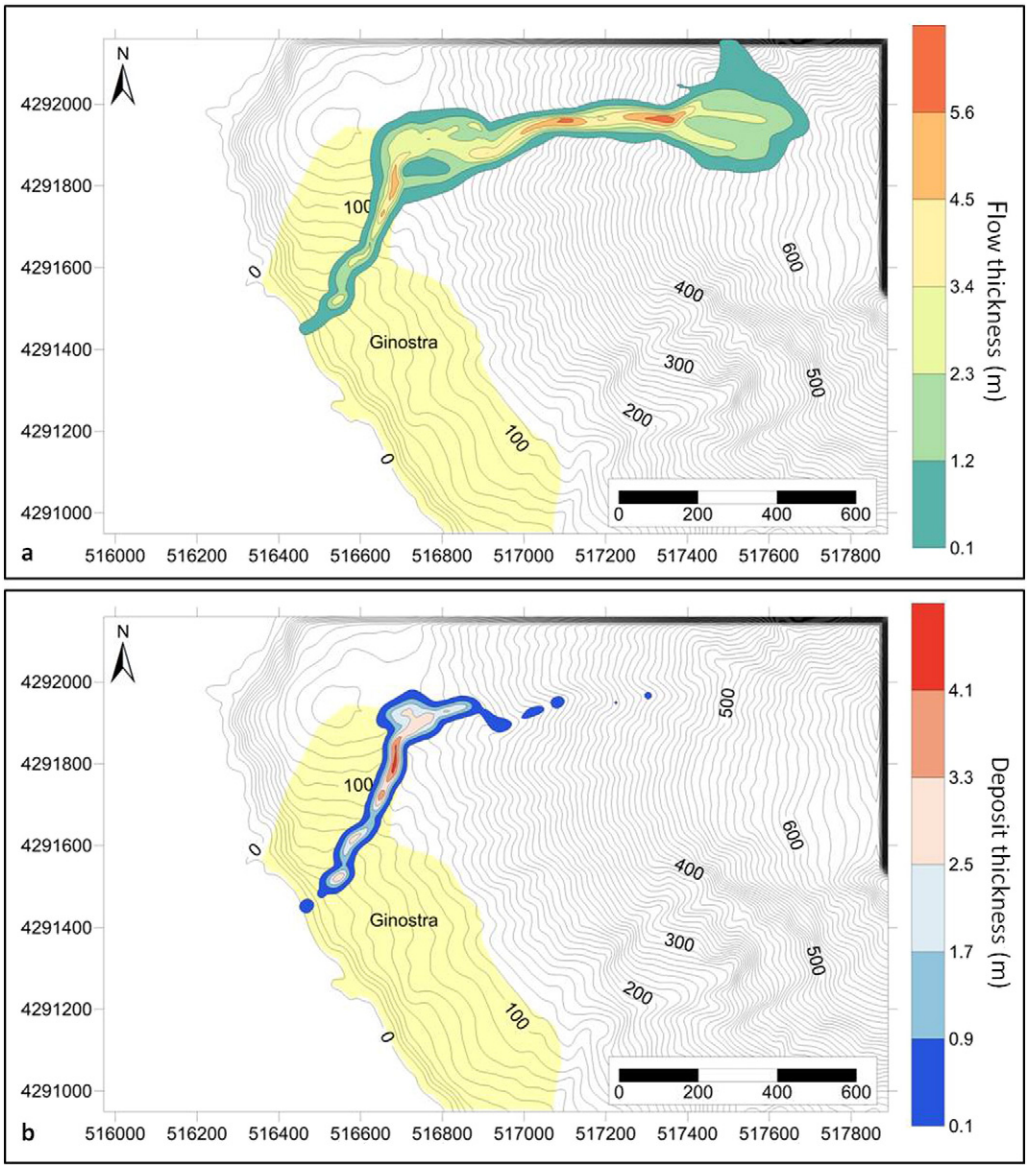

Fig. 9. Results of the DAN-3D simulation with a double input thickness: a) flow thickness and b) deposit thickness after an interval of 100 s for zone C (1906-like event).

Since the work of Hayashi and Self (1992), the assumption of a pure frictional internal rheology has been questioned based on observations of high mobility PDCs and volcanic debris avalanches. Long run-out rockfalls, debris avalanches and PDCs exhibit horizontal runout distances (L) that can be 5–20 times the vertical fall height (H), depending on the magnitude of the event. Several explanations for the scale dependence of H/L have been offered (Hungr, 1990), including mechanical fluidization (Hayashi and Self, 1992), acoustic fluidization (Melosh, 1979), and self-lubrication (Campbell, 1989). In particular, self-lubrification implies that most of the flowing mass moves over a thin, dilute layer of very agitated particles, where the energy dissipation is much smaller than in the mechanical fluidization (Hayashi and Self, 1992). Because this assumption was confirmed by the presence of a basal layer in the PDCs' deposits and the similarity of the basic physical processes that characterize dry granular avalanches and granular-flow dominated volcaniclastic flows (dense PDCs and debris avalanches), numerical codes that separate internal and basal frictions (i.e., Titan2D; Patra et al., 2005) have been increasingly used for reproducing past flows and hazard mapping (Saucedo et al., 2005; Norini et al., 2009; Widiwijayanti et al., 2009; Procter et al., 2010; Sulpizio et al., 2010b; Charbonnier and Gertisser, 2012).

DAN-3D was previously used by Morelli et al. (2010) and Sosio et al. (2012a) to constrain the flow parameters of large volcanic debris avalanches. Good results were obtained using DAN-3D for the large volume mass flows as well as the small-volume mass-flows investigated in this study. DAN-3D can be successfully used for modelling mass granular flows that are dominated by grain-collisions.

The main limitation of DAN-3D is the unchangeable internal rheology. Motion and field-based observations of dense PDCs and volcanic debris avalanche deposits have sometimes been explained using a plastic rheology (constant retarding stress or a Bingham rheology with no viscosity), in which the shear stress is constant regardless of the thickness or velocity of the flow (Dade and Huppert, 1998). Kelfoun and Druitt (2005) and Kelfoun et al. (2009, 2011) showed that the plastic rheology allows the morphology, lithology distribution and extension of volcanic debris avalanches and PDCs, even if Bingham behaviour with a minor viscous response cannot be excluded.

Charbonnier and Gertisser (2012) compared the hazard mapping of PDCs using both Titan2D (internal-basal frictional rheology) and VolcFlow (constant retarding stress). Their results evidenced the main limitation of using internal-basal frictional rheology for reproducing

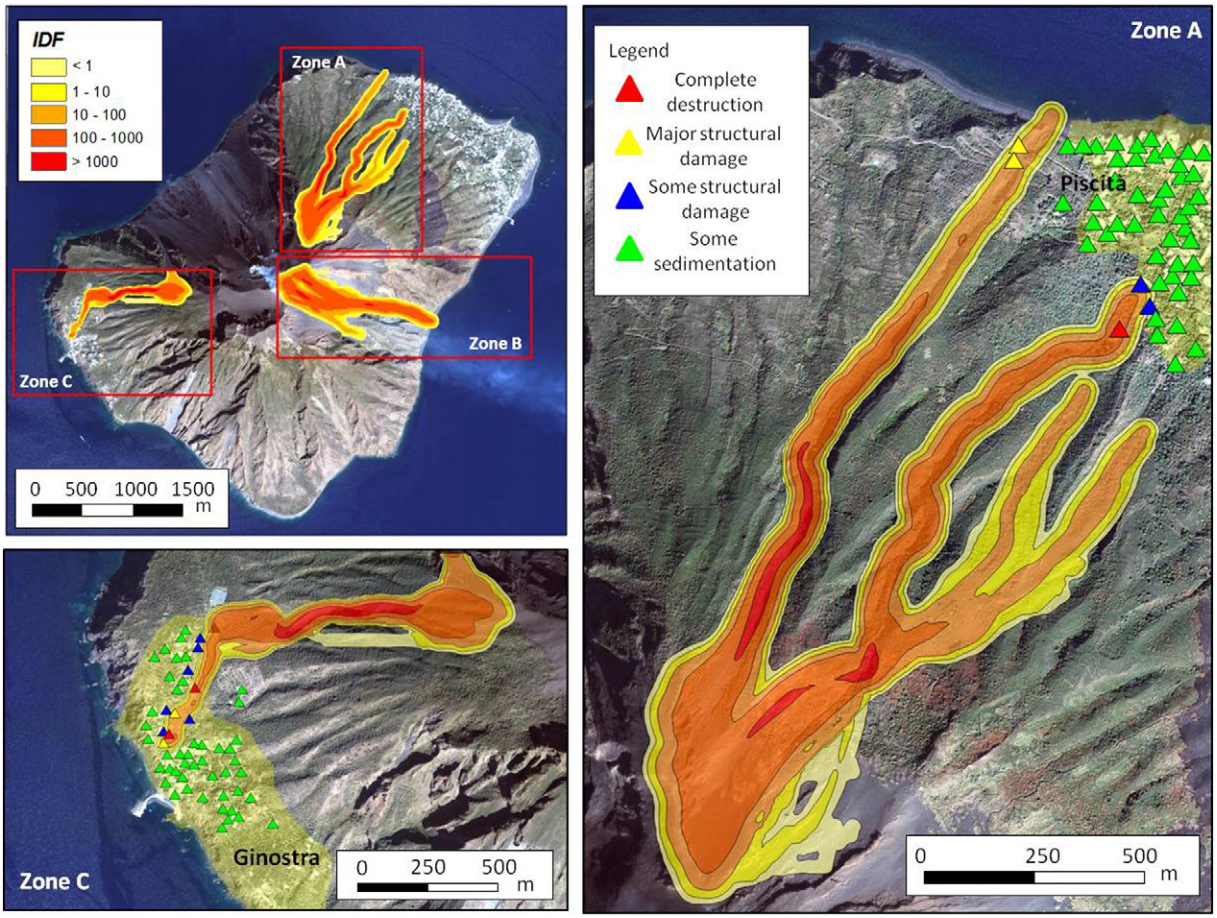

Fig. 10. Hazard evaluation for gravity-induced PDCs with the non-modified input thickness, showing the potential intensity index (I_{DF}) and the effect on buildings in the village of Stromboli, Piscità (zone A) and in the village of Ginostra (zone C).

PDC velocities and travel times. Using a constant retarding stress, the resulting simulations reproduced the morphologies and distributions of the natural deposits as well as the times of emplacement and velocities of the PDCs. Further investigations of the suitability of different internal rheologies will be performed.

5.2. Implications for hazards

The hazards at Stromboli can be related to different volcanic phenomena that include: ballistic fallout, tephra fallout, column-collapse or gravity-induced pyroclastic density currents, shockwaves, wildfires, lava flows and landslides and resultant tsunamis (Barberi et al., 1993; Rosi et al., accepted for publication). Hazardous volcanic events related to persistent activity are grouped into two categories: (1) moderately hazardous, relatively frequent events (1–2 per year), which include the fallout of heavy materials onto pathways and shelters generally used by guides and tourists and the ignition of wildfires; and (2) highly hazardous, medium frequency phenomena (a few events per century), which potentially can affect settled areas and include falling blocks that reach settled areas, PDCs, widespread wildfires and small tsunamis (Rosi et al., accepted for publication).

As mentioned, gravity-induced PDCs are usually confined to the Sciara del Fuoco depression and are produced by the remobilization of significant thicknesses of tephra on steep slopes during paroxysmal explosions, the collapse of the crater rims or by lava breaking off the sides and fronts of advancing lava flows (Pioli et al., 2008; Rosi et al., accepted for publication; Di Roberto et al., 2014; Di Traglia et al., 2014). Otherwise, small-volume gravity-induced PDCs were produced on the ESE side of the island in 1944, and on the inhabited NE part of the island in 1930 where they caused four casualties.

Hazard maps at the Stromboli volcano have been proposed by Barberi et al. (1993); Nave et al. (2010) and Rosi et al. (accepted for publication) and mainly focused on ballistic ejection and tsunamis, whereas threats associated with gravity-induced PDCs have not been examined in detail. This study represents the first contribution to a hazard assessment related to gravity-induced PDCs on Stromboli Island.

The potential damage from PDCs interacting with buildings in the villages of Stromboli and Ginostra was evaluated using the method proposed by Jakob et al. (2011), which has been applied to the evaluation of debris flow impacts. The method determines the potential building damage using an intensity index (I_{DF}; a sort of impact force):

$$I_{DF} = dv^2 \tag{4}$$

where d is the maximum expected flow depth, and v is the maximum flow velocity.

The dynamic pressure (P_{dyn}) used to estimate the potential impact of PDCs is defined as (Valentine, 1998):

$$P_{dyn} = 0.5\rho v^2 \tag{5}$$

where ρ is the flow density. Otherwise, in the dynamic pressure calculation, the particle concentrations, and the flow density are not always constrained. For the intensity index used here, only parameters derived from the modelling results were used; therefore, no other assumptions were made.

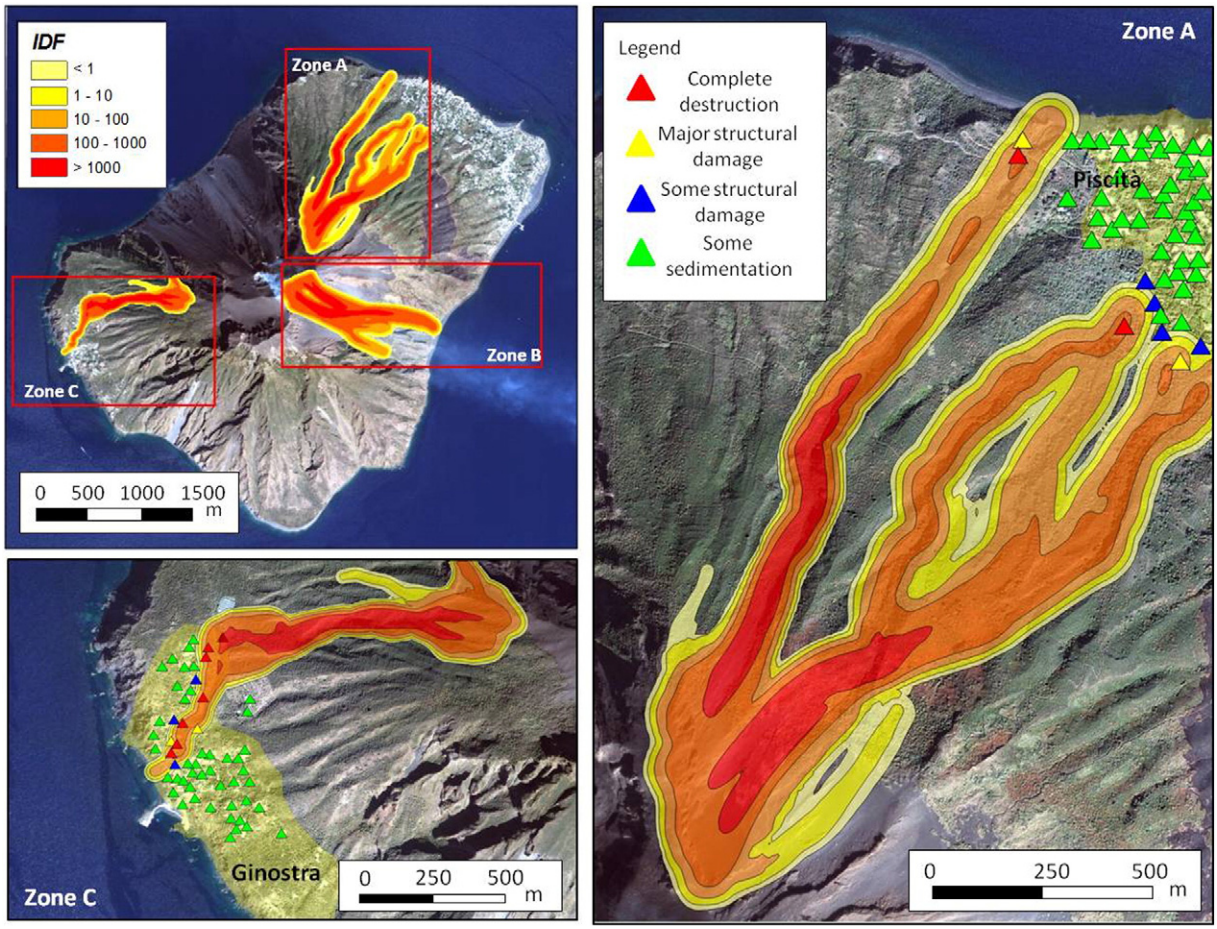

Fig. 11. Hazard evaluation for gravity-induced PDCs, with a double input thickness, showing the potential intensity index (I_{DF}) and the effect on buildings in the village of Stromboli, Piscità (zone A) and in the village of Ginostra (zone C).

The potential building damage was then estimated by classifying the calculated I_{DF} index, using the four classes proposed by Jakob et al. (2011), which range from some sedimentation (I) to complete destruction (IV). This classification is derived from back-analyses using building damage data from several case studies (Jakob et al., 2011; Corominas et al., 2014).

The modelling results in zone A were employed to evaluate the potential hazard in the Piscità zone of the village of Stromboli (Fig. 10). The simulations showed serious threats due to the flows channelled into the St. Bartolo and Vallonazzo valleys. The first flow could destroy and inflict structural damage to buildings in the village near the St. Bartolo Church, whereas the second flow could inflict major structural damage on two edifices on the Vallonazzo rims. The simulation carried out for zone C also revealed a potential hazard in the village of Ginostra (Fig. 10). The simulated path of the gravity-induced PDC, which travelled from the southwestern part of the summit area, could interact with the present-day urbanization of the village and result in some structural damage or the complete destruction of several buildings in the central part of Ginostra.

The simulations with double initial thicknesses of the sliding masses in zones A and C show that in the case of gravity-induced PDCs, the areas with higher I_{DF} would greatly increase (Fig. 11). This implies that the greater spatter accumulation in the upper part of the island is related to directed paroxysmal explosions, which could produce serious threats to the inhabited areas of the island. Zone B is free of human settlement and was not considered for this type of evaluation.

The results of the simulations with a double initial thicknesses suggest that the performance of DAN-3D for simulating events primarily depends on calibration using field-based data such as deposit distributions (locations and areas of initial piles) and volumes (single or multiple volumes), and direct observations (i.e., travel times).

6. Conclusions

Gravity-induced PDCs are well known for their ability to travel long distances, and understanding their mobility is therefore critical for evaluating areas at risk (Davies et al., 1978). Gravity-induced PDCs at the Stromboli volcano were analysed using the DAN-3D numerical code developed by McDougall and Hungr (2004) and Hungr and McDougall (2009) to reproduce the 1930 PDC extension and thickness reported in the literature. The best-fit results were obtained using a Voellmy model with a frictional coefficient $f = 0.19$ and a turbulence parameter $\xi = 1000\ \mathrm{m\ s^{-2}}$.

Hazard maps can be generated using DAN-3D. The potential damage from the gravity-induced PDCs was evaluated using the intensity index (I_{DF}) proposed by Jakob et al. (2011). The results showed that gravity-induced PDCs represent a serious threat and can potentially produce destruction and structural damage in all the inhabited areas of the Island of Stromboli. Moreover, the flow speed, number of impacted buildings, and the area with high I_{DF} values increase as the volumes of gravity-induced PDCs increase. Further investigations on the effects of this type of mass-wasting phenomena entering the sea are necessary to evaluate the tsunamigenic potential of the Stromboli gravity-induced PDCs.

DAN-3D has been used to constrain the flow parameters of large volcanic debris avalanches (Morelli et al., 2010, Sosio et al., 2012a) and the large-volume end-members of gravity-induced mass-flows in volcanic areas. The results obtained using DAN-3D for both small mass-flows

(this work) and the previously reported large mass-flows allow us to conclude that the model can be used for granular flows with various sizes, and can also be applied to other volcanoes prone to mass flows.

Acknowledgements

This work has been partially financed by the "Presidenza del Consiglio dei Ministri – Dipartimento della Protezione Civile" (Presidency of the Council of Ministers, Department of Civil Protection, Italy) in the framework of the InGrID and InGrID2015 research agreements between the Presidency of the Council of Ministers, Department of Civil Protection, and the Department of Earth Sciences, University of Firenze. This publication, however, does not reflect the position or official policies of the Department of Civil Protection. Karim Kelfoun, Jonathan Procter and an anonymous reviewer are thanked for their helpful comments, which have improved this manuscript, and we are grateful for valuable guidance from the editor, Takashi Oguchi.

References

Abbruzzese, D., 1935. Sulla catastrofica esplosione dello Stromboli dell'11 settembre 1930. Gioenia Proc. Soc. Nat. Sci 1, 1–13.

Alvarado, G.E., Soto, G.J., 2002. Pyroclastic flow generated by crater- wall collapse and outpouring of the lava pool of Arenal Volcano, Costa Rica. Bull. Volcanol. 63 (8), 557–568. http://dx.doi.org/10.1007/s00445-001-0179-9.

Apuani, T., Corazzato, C., Cancelli, A., Tibaldi, A., 2005a. Physical and mechanical properties of rock masses at Stromboli: a dataset for volcano instability evaluation. Bull. Eng. Geol. Environ. 64 (4), 419–431. http://dx.doi.org/10.1007/s10064-005-0007-0.

Apuani, T., Corazzato, C., Cancelli, A., Tibaldi, A., 2005b. Stability of a collapsing volcano (Stromboli, Italy): limit equilibrium analysis and numerical modelling. J. Volcanol. Geotherm. Res. 144 (1–4), 191–210. http://dx.doi.org/10.1016/j.jvolgeores.2004.11.028.

Aramaki, S., Takahashi, M., 1992. Geology and petrology of Asama Volcano. Field Workshop Guidebook to Asama and Kusatsu-Shirane Volcanoes, Japan. IAVCEI Commission on Explosive Volcanism.

Arrighi, S., Principe, C., Rosi, M., 2001. Violent strombolian and subplinian eruptions at Vesuvius during post-1931 activity. Bull. Volcanol. 63 (2–3), 126–150 (Doi: 10.1007ls004450100130).

Bagnold, R.A., 1954. Experiments on a gravity-free dispersion of large solid spheres in a Newtonian fluid under shear. Proceedings of the Royal Society of London A: Mathematical, Physical and Engineering Sciences. The Royal Society vol. 225(1160), pp. 49–63. http://dx.doi.org/10.1098/rspa.1954.0186.

Barberi, F., Rosi, M., Sodi, A., 1993. Volcanic hazard assessment at Stromboli based on review of historical data. Acta Vulcanol. 3, 173–187.

Behncke, B., Calvari, S., Giammanco, S., Neri, M., Pinkerton, H., 2008. Pyroclastic density currents resulting from the interaction of basaltic magma with hydrothermally altered rock: an example from the 2006 summit eruptions of Mount Etna, Italy. Bull. Volcanol. 70 (10), 1249–1268. http://dx.doi.org/10.1007/s00445-008-0200-7.

Benz, W., 1990. Smooth particle hydrodinamics: a review. In: Buchler, J.R. (Ed.), The Numerical Modelling of Nonlinear Stellar Pulsation. Kluwer Accademic, Dordrecht, pp. 269–288.

Bertagnini, A., Di Roberto, A., Pompilio, M., 2011. Paroxysmal activity at Stromboli: lessons from the past. Bull. Volcanol. 73 (9), 1229–1243. http://dx.doi.org/10.1007/s00445-011-0470-3.

Bonforte, A., Guglielmino, F., 2015. Very shallow dyke intrusion and potential slope failure imaged by ground deformation: the 28 December 2014 eruption on Mount Etna. Geophys. Res. Lett. 42 (8), 2727–2733.

Bursik, M., Patra, A., Pitman, E.B., Nichita, C., Macias, J.L., Saucedo, R., Girina, O., 2005. Advances in studies of dense volcanic granular flows. Rep. Prog. Phys. 68 (2), 271.

Calder, E.S., Cole, P.D., Dade, W., Druitt, T.H., Hoblitt, R.P., Huppert, H.E., Ritchie, L., Sparks, R.S.J., Young, S.R., 1999. Mobility of pyroclastic flows and surges at the Soufriere Hills Volcano, Montserrat. Geophys. Res. Lett. 26 (5), 537–540.

Calvari, S., Pinkerton, H., 2002. Instabilities in the summit region of Mount Etna during the 1999 eruption. Bull. Volcanol. 63, 526–535. http://dx.doi.org/10.1007/s004450100171.

Calvari, S., Intrieri, E., Di Traglia, F., Bonaccorso, A., Casagli, N., Cristaldi, A., 2016. Monitoring crater-wall collapse at active volcanoes: a study of the 12 January 2013 event at Stromboli. Bull. Volcanol. 78 (5), 1–16. http://dx.doi.org/10.1007/s00445-016-1033-4.

Campbell, C.S., 1989. Self-lubrication for long runout landslides. J. Geol. 653-665.

Charbonnier, S.J., Gertisser, R., 2012. Evaluation of geophysical mass flow models using the 2006 block-and-ash flows of Merapi Volcano, Java, Indonesia: towards a short-term hazard assessment tool. J. Volcanol. Geotherm. Res. 231, 87–108.

Chow, V.T., 1959. Open-channel Hydraulics. vol. 680. McGraw-Hill, New York.

Cole, P.D., Calder, E.S., Sparks, R.S.J., Clarke, A.B., Druitt, T.H., Young, S.R., Herd, R.A., Harford, C.L., Norton, G.E., 2002. Deposits from dome-collapse and fountain-collapse pyroclastic flows at Soufriere Hills Volcano. Montserrat. In: Druitt, T.H., Kokelaar, B.P. (Eds.), The Eruption of Soufriere Hills Volcano, Montserrat, From 1995 to 1999. Geological Society, London. Memoirs vol. 21, pp. 231–262.

Cole, P.D., Fernandez, E., Duarte, E., Duncan, A.M., 2005. Explosive activity and generation mechanisms of pyroclastic flows at Arenal volcano, Costa Rica between 1987 and 2001. Bull. Volcanol. 67 (8), 695–716. http://dx.doi.org/10.1007/s00445-004-0402-6.

Corominas, J., Van Westen, C., Frattini, P., Cascini, L., Malet, J.P., Fotopoulou, S., Catani, F., Van Den Eeckhaut, M., Mavrouli, O., Agliardi, F., Pitilakis, K., Winter, M.G., Pastor, M., Ferlisi, S., Tofani, V., Herva's, J., Smith, J.T., 2014. Recommendations for the quantitative analysis of landslide risk. Bull. Eng. Geol. Environ. 73 (2), 209–263.

Coulomb, C.A., 1776. Sur une application des regles maximis et minimis a quelques problems de statique, relatives a l'architec-ture. Acad. Sci. Paris Mem. Math. Phys. 7, 343–382.

Dade, W.B., Huppert, H.E., 1998. Long runout rockfalls. Geology 26, 803–806.

Davies, K.D., Quearry, M.W., Bonis, S.B., 1978. Glowing avalanches from the 1974 eruption of the volcano Fuego, Guatemala. Geol. Soc. Am. Bull. 89, 369–384. http://dx.doi.org/10.1130/0016-7606(1978)89<369:GAFTEO>2.0.CO;2.

De Beni, E., Behncke, B., Branca, S., Nicolosi, I., Carluccio, R., Caracciolo, F.A., Chiappini, M., 2015. The continuing story of Etna's New Southeast Crater (2012–2014): evolution and volume calculations based on field surveys and aerophotogrammetry. J. Volcanol. Geotherm. Res. 303, 175–186.

De Fino, M., La Volpe, L., Falsaperla, S., Frazzetta, G., Neri, G., Francalanci, L., Rosi, M., Sbrana, A., 1988. The Stromboli eruption of December 6, 1985–April 25, 1986: volcanological, petrological and seismological data. Rend. Soc. Ital. Mineral. Petrol. 43, 1021–1038.

Di Roberto, A., Bertagnini, A., Pompilio, M., Bisson, M., 2014. Pyroclastic density currents at Stromboli volcano (Aeolian Islands, Italy): a case study of the 1930 eruption. Bull. Volcanol. 76 (6), 1–14. http://dx.doi.org/10.1007/s00445-014-0827-5.

Di Traglia, F., Intrieri, E., Nolesini, T., Bardi, F., Del Ventisette, C., Ferrigno, F., Frangioni, S., Frodella, W., Gigli, G., Lotti, A., Tacconi Stefanelli, C., Tanteri, L., Leva, D., Casagli, N., 2014. The ground-based InSAR monitoring system at Stromboli volcano: linking changes in displacement rate and intensity of persistent volcanic activity. Bull. Volcanol. 76, 1–18. http://dx.doi.org/10.1007/s00445-013-0786-2.

Hayashi, J.N., Self, S., 1992. A comparison of pyroclastic flow and debris avalanche mobility. J. Geophys. Res. 97B6, 9063–9071.

Hazlett, R.W., Buesch, D., Anderson, J.L., Elan, R., Scandone, R., 1991. Geology, failure conditions, and implications of seismogenic avalanches of the 1944 eruption at Vesuvius, Italy. J. Volcanol. Geotherm. Res. 47 (3–4), 249–264. http://dx.doi.org/10.1016/0377-0273(91)90004-J.

Heim, A., 1932. Bergsturz und Menschenleben. Zurich, Fretz und Wasmuth. English Translation by N.A. Skermer 1989 Landslide and Human Lives. BiTech Publusher, Vancouver B.C.

Hungr, O., 1990. Mobility of rock avalanches: report of the National Research Institute of Earth Science and Disaster Prevention, Japan. 46, 11–20.

Hungr, O., 1995. A model for the runout analysis of rapid flow slides, debris flows, and avalanches. Can. Geotech. J. 32, 610–623.

Hungr, O., McDougall, S., 2009. Two numerical models for landslide dynamic analysis. Comput. Geosci. 35 (5), 978–992. http://dx.doi.org/10.1016/j.cageo.2007.12.003.

Hungr, O., Leroueil, S., Picarelli, L., 2014. The Varnes classification of landslide types, an update. Landslides 11, 167–194.

Iverson, R.M., Denlinger, R.P., 2001. Flow of variably fluidized granular masses across three-dimensional terrain: 1. Coulomb mixture theory. J. Geophys. Res. Solid Earth 106 (B1), 537–552. http://dx.doi.org/10.1029/2000JB900329.

Jakob, M., Stein, D., Ulmi, M., 2011. Vulnerability of buildings to debris flow impact. Nat. Hazards 60, 241–261. http://dx.doi.org/10.1007/s11069-011-0007-2.

Kelfoun, K., 2011. Suitability of simple rheological laws for the numerical simulation of dense pyroclastic flows and long-runout volcanic avalanches. J. Geophys. Res. Solid Earth 116 (B8).

Kelfoun, K., Druitt, T.H., 2005. Numerical modeling of the emplacement of Socompa rock avalanche, Chile. J. Geophys. Res. Solid Earth 110 (B12), 1978–2012.

Kelfoun, K., Samaniego, P., Palacios, P., Barba, D., 2009. Testing the suitability of frictional behaviour for pyroclastic flow simulation by comparison with a well-constrained eruption at Tungurahua volcano (Ecuador). Bull. Volcanol. 71, 1057–1075.

Kelfoun, K., Giachetti, T., Labazuy, P., 2010. Landslide-generated tsunamis at Réunion Island. J. Geophys. Res. Earth Surf. 115 (F4). http://dx.doi.org/10.1029/2009JF001381.

Lube, G., Cronin, S.J., Platz, T., Freundt, A., Procter, J.N., Henderson, C., Sheridan, M.F., 2007. Flow and deposition of pyroclastic granular flows: a type example from the 1975 Ngauruhoe eruption, New Zealand. J. Volcanol. Geotherm. Res. 161 (3), 165–186. http://dx.doi.org/10.1016/j.jvolgeores.2006.12.003.

McDougall, S., Hungr, O., 2003. Objectives for the development of an integrated three-dimensional continuum model for the analysis of landslide runout. In: Rickenmann, D., Chen, C.L. (Eds.), Proceedings of the 3rd Inter-national Conference on Debris-flow Hazards Mitigation: Mechanics, Prediction and Assessment. Millpress, Rotterdam, The Netherlands, pp. 481–490.

McDougall, S., Hungr, O., 2004. A model for the analysis of rapid landslide motion across three-dimensional terrain. Can. Geotech. J. 41 (6), 1084–1097. http://dx.doi.org/10.1139/T04-052.

Melosh, H.J., 1979. Acoustic fluidization: a new geologic process? J. Geophys. Res. Solid Earth 84 (B13), 7513–7520. http://dx.doi.org/10.1029/JB084iB13p07513.

Miyabuchi, Y., Ikebe, S.I., Watanabe, K., 2005. The July 10, 2003 and the January 14, 2004 ash emissions from a hot water pool of the Nakadake crater, Aso volcano, Japan. Bull. Volcanol. Soc. Jpn. 50, 227–241.

Miyabuchi, Y., Watanabe, K., Egawa, Y., 2006. Bomb-rich basaltic pyroclastic flow deposit from Nakadake, Aso Volcano, southwestern Japan. J. Volcanol. Geotherm. Res. 155 (1–2), 90–103. http://dx.doi.org/10.1016/j.jvolgeores.2006.02.007.

Monaghan, J.J., 1989. On the problem of penetration in particle methods. J. Comput. Phys. 82, 1–15.

Monaghan, J.J., 1992. Smoothed particle hydrodynamics. Annu. Rev. Astron. Astrophys. 30, 543–574.

Morelli, S., Garduño Monroi, V.H., Gigli, G., Falorni, G., Arreygue Rocha, E., Casagli, N., 2010. The Tancitaro debris avalanche: characterization, propagation and modelling.

J. Volcanol. Geotherm. Res. 193, 93–105. http://dx.doi.org/10.1016/j.jvolgeores.2010.03.008.
Nairn, I.A., Self, S., 1978. Explosive eruptions and pyroclastic avalanches from Ngauruhoe in February 1975. J. Volcanol. Geotherm. Res. 3 (1–2), 39–60.
Nave, R., Ricci, T., Barberi, F., Davis, M., Isaia, R., 2010. Perception of volcanic risk in Italy: Etn, Vesuvio and Campi Flegrei. Cities on Volcanoes 6 Conference.
Nolesini, T., Di Traglia, F., Del Ventisette, C., Moretti, S., Casagli, N., 2013. Deformations and slope instability on Stromboli volcano: integration of GBInSAR data and analog modelling. Geomorphology 180, 242–254.
Norini, G., De Beni, E., Andronico, D., Polacci, M., Burton, M., Zucca, F., 2009. The 16 November 2006 flank collapse of the south-east crater at Mount Etna, Italy: study of the deposit and hazard assessment. J. Geophys. Res. Solid Earth 114 (B2) 1978–2012.
Patra, A.K., Bauer, A.C., Nichita, C.C., EPitman, E.B., Sheridan, M.F., Bursik, M., Rupp, B., Webber, A., Stinton, A.J., Namikawa, L.M., Renschler, C.S., 2005. Parallel adaptive numerical simulation of dry avalanches over natural terrain. J. Volcanol. Geotherm. Res. 139 (1–2), 89–102. http://dx.doi.org/10.1007/s11069-009-9440-x.
Pioli, L., Rosi, M., Calvari, S., Spampinato, L., Renzulli, A., Di Roberto, A., 2008. The Eruptive Activity of 28 and 29 December 2002, the Stromboli Volcano an Integrated Study of the 2002–2003 Eruption. American Geophysical Union, Washington, USA, pp. 105–115 http://dx.doi.org/10.1029/182GM10.
Pistolesi, M., Rosi, M., Pioli, L., Renzulli, A., Bertagnini, A., Andronico, D., 2008. The paroxysmal event and its deposits. In: Calvari, S., Inguaggiato, S., Puglisi, G., Ripepe, M., Rosi, M. (Eds.), The Stromboli Volcano an Integrated Study of the 2002–2003 Eruption. American Geophysical Union, Washington, USA, pp. 317–330.
Ponte, G., 1948. Attività straordinaria dello Stromboli. Ann. Geophys. 1 (2), 200–202.
Procter, J.N., Cronin, S.J., Platz, T., Patra, A., Dalbey, K., Sheridan, M., Neall, V., 2010. Mapping block-and-ash flow hazards based on Titan 2D simulations: a case study from Mt. Taranaki, NZ. Nat. Hazards 53 (3), 483–501.
Riccò, A., 1907. Sull'attività dello Stromboli dal 1891 in poi. Boll. Soc. Sismol. Ital. 12, 205.
Rittmann, A., 1931. Der Ausbruch des Stromboli am 11. September 1930. Z Vulkanologie 14, 47–77.
Rosi, M., Bertagnini, A., Landi, P., 2000. Onset of the persistent activity at Stromboli volcano (Italy). Bull. Volcanol. 62 (4–5), 294–300.
Rosi, M., Bertagnini, A., Harris, A.J.L., Pioli, L., Pistolesi, M., Ripepe, M., 2006. A case history of paroxysmal explosion at Stromboli: timing and dynamics of the April 5, 2003 event. Earth Planet. Sci. Lett. 243 (3), 594–606. http://dx.doi.org/10.1016/j.epsl.2006.01.035.
Rosi, M., Pistolesi, M., Bertagnini, A., Landi, P., Pompilio, M., Di Roberto, A., 2013. Stromboli Volcano, Aeolian Islands (Italy): present eruptive activity and hazard. In: Lucchi, F., Peccerillo, A., Keller, J., Tranne, C.A., Rossi, P.L. (Eds.), Geol. Soc. London Mem., Geology of the Aeolian Islands (Italy) (accepted for publication).
Saucedo, R., Macıas, J.L., Sheridan, M.F., Bursik, M.I., Komorowski, J.C., 2005. Modelling of pyroclastic flows of Colima Volcano, Mexico: implications for hazard assessment. J. Volcanol. Geotherm. Res. 139, 103–115. http://dx.doi.org/10.1016/j.jvolgeores.2004.06.019.
Savage, S.B., Hutter, K., 1989. The motion of a finite mass of granular material down a rough incline. J. Fluid Mech. 199, 177–215.
Sosio, R., Crosta, G.B., Hungr, O., 2008. Complete dynamic modelling calibration for the Thurwieser rock avalanche (Italian Central Alps). Eng. Geol. 100, 11–26. http://dx.doi.org/10.1016/j.enggeo.2008.02.012.
Sosio, R., Crosta, G.B., Hungr, O., 2012a. Numerical modelling of debris avalanche propagation from collapse of volcanic edifices. Landslides 9, 315–334. http://dx.doi.org/10.1007/s10346-011-0302-8.
Sosio, R., Crosta, G.B., Chen, J.H., Hungr, O., 2012b. Modelling rock avalanche propagation onto glaciers. Quat. Sci. Rev. 47, 23–40.
Sulpizio, R., Bonasia, R., Dellino, P., Mele, D., Di Vito, M.A., La Volpe, L., 2010a. The Pomici di Avellino eruption of Somma–Vesuvius (3.9 ka BP). Part II: sedimentology and physical volcanology of pyroclastic density current deposits. Bull. Volcanol. 72 (5), 559–577. http://dx.doi.org/10.1007/s00445-009-0340-4.
Sulpizio, R., Capra, L., Sarocchi, D., Saucedo, R., Gavilanes-Ruiz, J.C., Varley, N.R., 2010b. Predicting the block-and-ash flow inundation areas at Volcán de Colima (Colima, Mexico) based on the present day (February 2010) status. J. Volcanol. Geotherm. Res. 193 (1), 49–66.
Takahashi, T., Tsujimoto, H., 2000. A mechanical model for Merapi-type pyroclastic flow. J. Volcanol. Geotherm. Res. 98 (1), 91–115. http://dx.doi.org/10.1016/S0377-0273(99)00193-6.
Ui, T., Matsuwo, N., Sumita, M., Fujinawa, A., 1999. Generation of block-and-ash flows during the 1990–1995 eruption of Unzen Volcano, Japan. J. Volcanol. Geotherm. Res. 89, 123–137. http://dx.doi.org/10.1016/S0377-0273(98)00128-0.
Valentine, G.A., 1998. Damage to structures by pyroclastic flows and surges, inferred from nuclear weapons effects. J. Volcanol. Geotherm. Res. 87 (1), 117–140.
Widiwijayanti, C., Voight, B., Hidayat, D., Schilling, S.P., 2009. Objective rapid delineation of areas at risk from block-and-ash pyroclastic flows and surges. Bull. Volcanol. 71 (6), 687–703. http://dx.doi.org/10.1007/s00445-008-0254-6.
Yamamoto, T., Takada, A., Ishizuka, Y., Miyaji, N., Tajima, Y., 2005. Basaltic pyroclastic flows of Fuji volcano, Japan: characteristics of the deposits and their origin. Bull. Volcanol. 67 (7), 622–633. http://dx.doi.org/10.1007/s00445-004-0398-y.
Yasui, M., Koyaguchi, T., 2004. Sequence and eruptive style of the 1783 eruption of Asama Volcano, central Japan: a case study of an andesitic explosive eruption generating fountain-fed lava flow, pumice fall, scoria flow and forming a cone. Bull. Volcanol. 66 (3), 243–262.